Philosophical Magazine, 1 Nov–1 Dec 2003
Vol. 83, Nos. 31–34, 3609–3622

Taylor & Francis
Taylor & Francis Group

Dislocation nucleation in the initial stage during nanoindentation

H. Y. Liang, C. H. Woo†

Department of Mechanical Engineering, Hong Kong Polytechnic University, Hong Kong SAR, China

Hanchen Huang

Department of Mechanical, Aerospace and Nuclear Engineering, Rensselaer Polytechnic Institute, Troy, New York 12180, USA

A. H. W. Ngan

Department of Mechanical Engineering, University of Hong Kong, Hong Kong SAR, China

and T. X. Yu

Department of Physics, Hong Kong University of Science and Technology, Hong Kong SAR, China

[*Received 17 June 2002 and in final form 27 May 2003*]

Abstract

The microstructure origin of the elastic–plastic response of a Cu substrate during nanoindentation is studied using molecular dynamics simulation. The elastic response is found to deviate from the Hertzian solution observed experimentally. The departure can be traced to the small tip radius used in the simulation. Further penetration sees the development of an inhomogeneous microstructure. Even at the same strain rate, different parts of the contact surface deform via different mechanisms: some elastically, some via the dislocation bow-out and some via the nucleation and growth of Shockley partials that sometimes interact to form stair-rod locks. The resultant effect produces the observed quasi-elastic behaviour on the load–displacement curve, characterized by interspersed minor yields. The present computer simulation shows in some detail the corresponding dislocation structure development. The stair-rod lock formation is found to provide a more satisfactory explanation to the experimentally observed time-delayed occurrence of pop-in below the spontaneous pop-in load.

§1. Introduction

As the nanoscale counterpart of the traditional microhardness tests, nanoindentation can provide much more fundamental insight into the mechanical properties of

†Author for correspondence. Email: chung.woo@polyu.edu.hk.

Philosophical Magazine ISSN 1478–6435 print/ISSN 1478–6443 online
http://www.tandf.co.uk/journals
DOI: 10.1080/14786430310001605579

materials with atomic resolution. Indeed, during nanoindentation, the movement of even just a few dislocations can be detected directly, through the response of the indentation load. However, the interpretation of nanoindentation results is complex, because of the large number of dependent variables that affect the loading behaviour, such as the nature of the surface, the size and tip geometry of the indenter, the penetration depth, the crystallographic and elastic anisotropy, the thickness of the substrate and the strain gradient effects (Gouldstone *et al*. 2000, Gerberich *et al*. 2002, Swadener *et al*. 2002).

Two interesting observations have been confirmed by many nano-indentation experiments. Firstly, single crystals can sustain ultrahigh stresses approaching the theoretical shear strength. This phenomenon has been attributed to plasticity in a defect-free region, to a triaxial stress state that stabilizes the structure and raises the ideal strength in shear, or to surface effects (Gane and Bowden 1968, Krenn *et al*. 2002). It is often presumed that the substrate behaves elastically before the first plastic deformation takes place. However, the possibility of a pre-existing dislocation around the indenter cannot be excluded (Gane and Bowden 1968), and some dislocation movements may have already taken place well before the detection of the first major plastic response. Indeed, minor dislocation activities have been reported to appear in the Hertzian elastic stage by Kiely *et al*. (1999).

Secondly, plasticity during nano-indentation usually occurs as pop-in (in force-controlled experiments) or sudden force drop (in displacement-controlled experiments) phenomena, resulting probably from the nucleation, multiplication, motion and pile-up of dislocations, or phase transition (Gane and Bowden 1968, Corcoran *et al*. 1997, Kiely and Houston 1998, Kiely *et al*. 1999, Gouldstone *et al*. 2000). Interpretation of experimental results is complicated by the dominance of surface factors such as steps, asperities, oxides, contamination, or mechanical hardened surface regions (Kiely and Houston 1998, Kiely *et al*. 1998, Kramer *et al*. 2001, Liu and Ngan 2001). This is particularly the case during the very early stages of loading. Nevertheless, it appears that the rupture of the surface oxide layer is not a primary mechanism responsible for the displacement excursion (Gouldstone *et al*. 2000, Minor *et al*. 2001, Chiu and Ngan 2002). Discrete yielding events during nanoindentation have been observed by several workers on a clean single-crystal Au surface with a large flat terrace (Corcoran *et al*. 1997, Kiely and Houston 1998, Kiely *et al*. 1999). Recently, by recording the entire process of nanoindentation on film, Minor *et al*. (2001) found that the onset of plastic deformation is directly connected to the movement of dislocations initiated from the surface.

Despite a growing body of experimental studies, atomistic simulation studies still provide a large proportion of the information concerning the evolution of microstructure during nanoindentation, especially in the initial stage. Using molecular dynamics (MD) simulation, Kelchner *et al*. (1998) studied displacement-controlled indentation on an Au(111) surface and found that dislocation loops started to appear to one side of the indenter axis, when the applied shear stress reached 7 GPa, well above the critical shear stress level of 2 GPa. Zimmerman *et al*. (2001) investigated the effect of surface steps on dislocation nucleation under an indenter of tip radius of 4 nm and found a significant reduction in the required load, if applied next to the step. Rodríguez de la Fuente *et al*. (2002) studied the formation of hillocks near indentation points and found that they were composed of four Shockley partials and a stair-rod dislocation. More recently, the MD simulation results of Li *et al*. (2002) suggested that the incipient dislocation loops, which

were nucleated homogeneously at the gigapascal stress level, were only responsible for the minor relaxation. Acting as dislocation sources operating at the megapascal stress level, these then became responsible for most of the plastic behaviour.

In this paper, MD simulation of nanoindentation on a Cu(100) surface is performed, aiming to gain insight into the relationship between the displacement–load behaviour and the associated dislocation structure development.

§ 2. Simulation procedure and results

2.1. *Simulation procedure*

In the following, the embedded-atom method potential of Doyama *et al.* (1999) for Cu is adopted, with parameters determined from the experimental values of cohesive energy, Born stability, elastic constants C_{11}, C_{12} and C_{44}, formation energy of a vacancy and stacking-fault energy. The Cu substrate is a rectangular crystal lattice with dimensions 188 Å × 188 Å × 108 Å, containing 324 480 atoms (figure 1). The top surface of the substrate is the (001) crystal plane, and the other two side surfaces are (100) and (010) planes respectively. Periodic boundary conditions are applied to the two side faces. The top surface is traction free, and the two atom layers at the bottom are held fixed. The temperature of the simulation cell (i.e. all the moving atoms) is kept constant at 300 K through the Nosé–Hoover thermostat. Following Kelchner *et al.* (1998), a repulsive potential is used to model a spherical indenter of radius $R = 40$ Å, penetrating into a frictionless surface.

The indentation velocity is about 3 m s^{-1}, similar to that used by other workers, such as Christopher *et al.* (2001) who used a velocity of 40 m s^{-1}, and Gannepalli and Mallapragada (2002) who used a value of 50 m s^{-1}. This velocity is nine orders of magnitude higher than the experimental values, a necessary 'evil' due to the usual restrictions of MD in terms of both temporal and spatial scales. The sensitivity of the simulation results to the indentation velocity has to be considered before the simulation and experimental results can be directly compared. We found that, while a higher indentation velocity in MD simulation leads to a higher strength, the relationship between the applied load and the indentation depth remains relatively

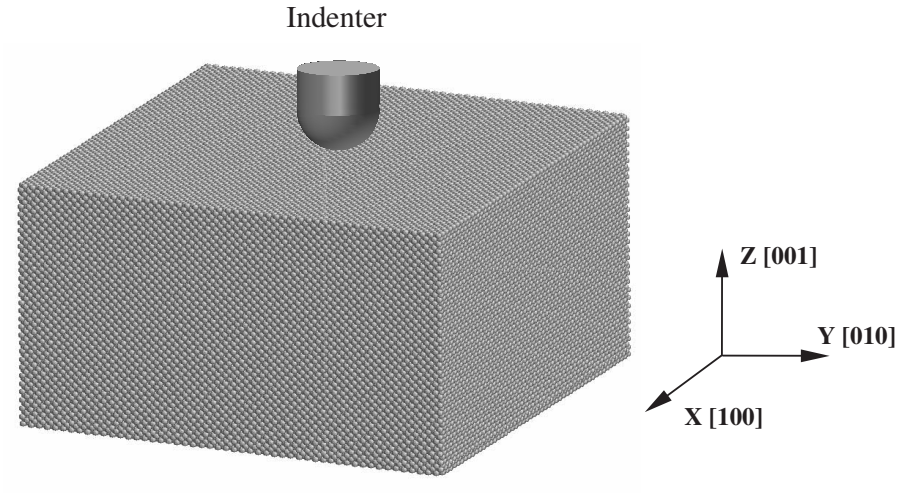

Figure 1. Schematic diagram of the simulation set-up for indentation on the Cu(100) surface.

unaffected. At the same time, the ensuing dislocation structures are also not substantially different. More importantly, the values will quickly converge as the velocity decreases and approach approximately $3\,\mathrm{m\,s^{-1}}$. In fact, no obvious difference is apparent when the velocity is below $3\,\mathrm{m\,s^{-1}}$. Nevertheless, we must be aware that convergence within MD here does not necessarily ensure that the effects of time-dependent mechanisms, such as diffusion-driven mechanisms, have been properly accounted for.

2.2. *Elastic regime*

The resulting indentation depth h is plotted as a function of the applied load F in the displacement–load curve in figure 2. As expected, for small indentation depths of less than 4.0 Å, the displacement–load curve exhibits a smooth elastic behaviour. However, in contrast with published experimental results, which normally follow the Hertzian relation $F \propto h^{3/2}$, our results in figure 2 do not. This can be understood because the Hertzian elastic solution requires the indentation depth h to be much smaller than the tip radius R (i.e. $h \ll R$), a condition that is not met in the present case. The Hertz model has to be corrected for the geometric nonlinearity before it can be considered for the case where $h \approx R$. Indeed, indentation experiments with tip radius ($R = 50$–250 Å) comparable with the penetration depth also found a deviation from Hertzian solution (Kracke and Damaschke 2000, Fraxedas *et al.* 2002). Replotting these experimental results, a relation of $F \propto h^n$, where $n \approx 1.9$, is obtained for a depth of less than 15 Å. This compares well with the relation

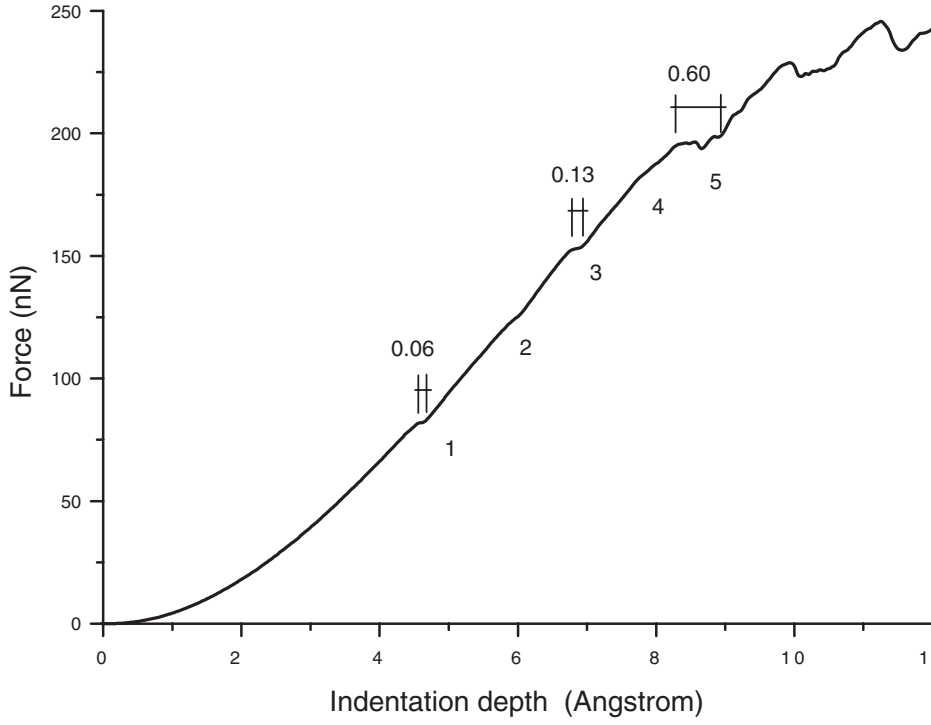

Figure 2. Load–displacement curve plotting indentation depth h as a function of applied load F, from the MD simulation.

$F \propto h^{1.85}$ in the present case obtained by fitting to the part of the displacement–load curve before point 1 in figure 2.

The contours of the displacement along the Z axis at a penetration depth of about 4.0 Å are shown in figure 3. This deformation behaviour is typical in the elastic stage prior to point 1. Figure 3 (*a*) shows the displacement of the atoms on the top surface X–Y. Figure 3 (*b*) shows the displacement contour on the cross-section (Y–Z plane) along the indenter axis ($X = 0$). Because of the elastic anisotropy of the fcc Cu substrate, the elastic displacement field is orientation dependent. Indeed, it can be seen in figure 3 (*b*) that the vertical atomic displacements a few atomic layers beneath the surface are not symmetrical with respect to the axis of the indenter,

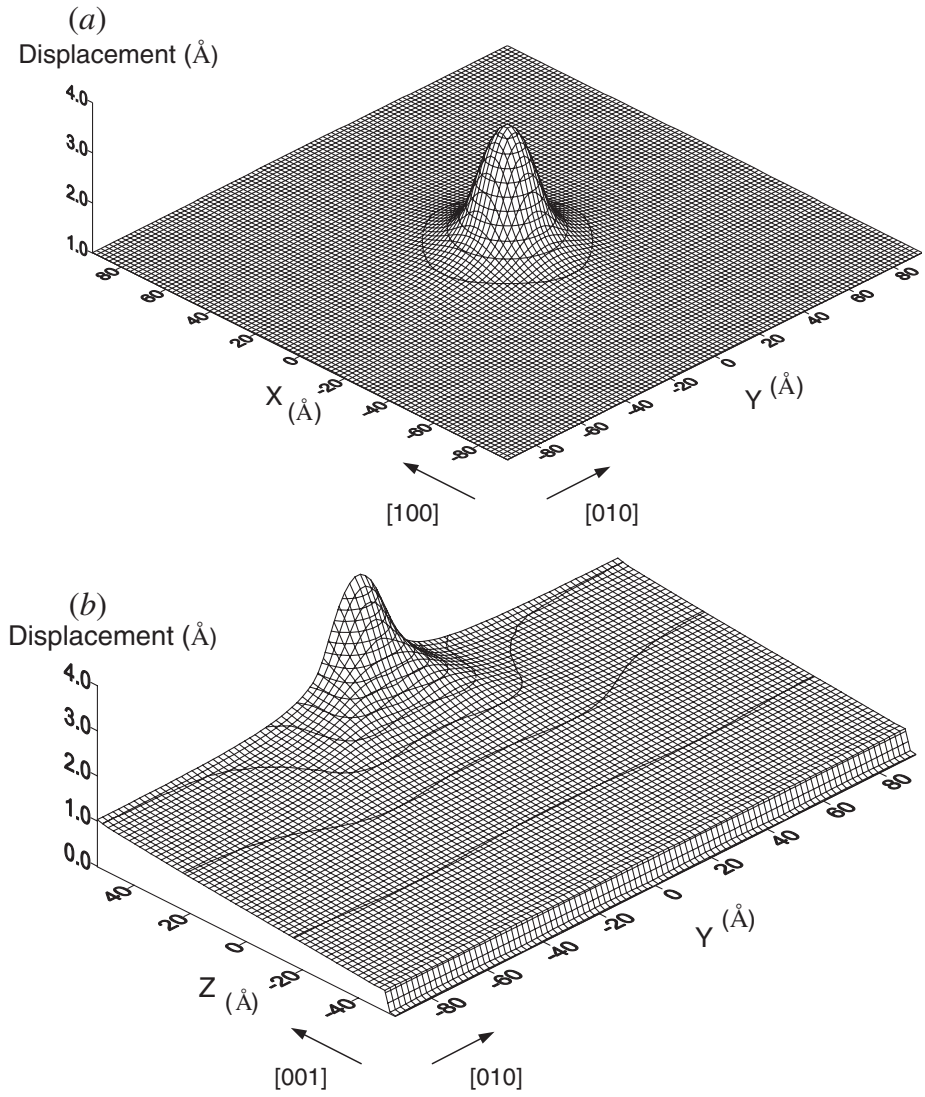

Figure 3. Contours of displacement (Z component) during the elastic stage at a penetration depth of 4.0 Å: (*a*) the displacement of atoms on the top surface; (*b*) the displacement contour on the cross section (Y–Z plane) along the indenter axis.

indicating larger shear stress off the indenter axis. From figure 3, it can also be seen that the stressed volume is sufficiently small relative to the simulation cell size.

2.3. *Incipient plasticity*

In the load–displacement curve in figure 2, there are five inflection points produced by minor yielding due to inelastic deformation under the indenter. Their occurrence suggests specific events in the development of the dislocation structure during the indentation. Between the inflection points, the curve shows a relatively stable and smooth deformation behaviour, suggesting the steady development of the incipient dislocation structure. The magnitude of the inelastic displacements at points 1, 3, and 5 are 0.06, 0.13 and 0.60 Å respectively, suggesting an increasing magnitude of the underlying dislocation activities. Beyond the load drop at point 5, large excursions appear frequently and the curve no longer has any smooth part, suggesting that the evolution of the dislocation structure has become more complex. We shall further discuss these observations in relation to the microstructure development during the indentation in the next few paragraphs.

For an increased radius of the tip, the number of atoms directly under the indenter also increases. As a result, the relative number of atoms involved in the nucleation and movement of individual dislocations will decrease, when averaged over all the atoms under the indenter, most of which are displaced only elastically. This may be the reason why minor dislocation events in the early stages of loading are not often observable experimentally (Kiely *et al.* 1999, Kramer *et al.* 2001). In our MD simulation, the size of the indenter is one to two orders of magnitude smaller than that used experimentally. The stressed volume beneath the indenter is sufficiently small that the number of atoms involved in the dislocation events constitutes a substantial percentage of the total. The dislocation events thus show up as minor yields in figure 2.

At this point, we note that the present simulation exercise has been repeated for Cu(111) and Cu(110) surfaces and, similar to the results of Kelchner *et al.* (1998) and Zimmerman *et al.* (2001), the load–displacement relation that we obtained also follows a smooth curve until a sudden large load drop, without the prior occurrence of minor yields such as those in figure 2.

2.4. *Microstructure development*

To correlate between the dislocation structure development beneath the indenter and the load–displacement behaviour, one needs to identify the details of dislocation structure. Several techniques are available, such as common neighbour analysis (Clarke and Jonsson 1993), atomic stress tensor (Kulp *et al.* 1993), Voronoi polyhedra analysis (Brostow *et al.* 1998), centrosymmetry parameter (Kelchner *et al.* 1998), and slip vector (Zimmerman *et al.* 2001). The slip vector, which is closely related to the Burgers vector, is adopted in the present paper to analyse the dislocation structures. A slip vector $\mathbf{s}^{\alpha}$ can be defined for each atom as

$$\mathbf{s}^{\alpha} = -\frac{1}{n_{\mathrm{s}}}\sum_{\beta\neq\alpha}^{n}(\mathbf{x}^{\alpha\beta} - \mathbf{X}^{\alpha\beta}), \tag{1}$$

where $\mathbf{x}^{\alpha\beta}$ and $\mathbf{X}^{\alpha\beta}$ are the vectors linking the atom α with all its nearest neighbours β in the current and reference positions, and n_{s} is the number of slipped neighbours.

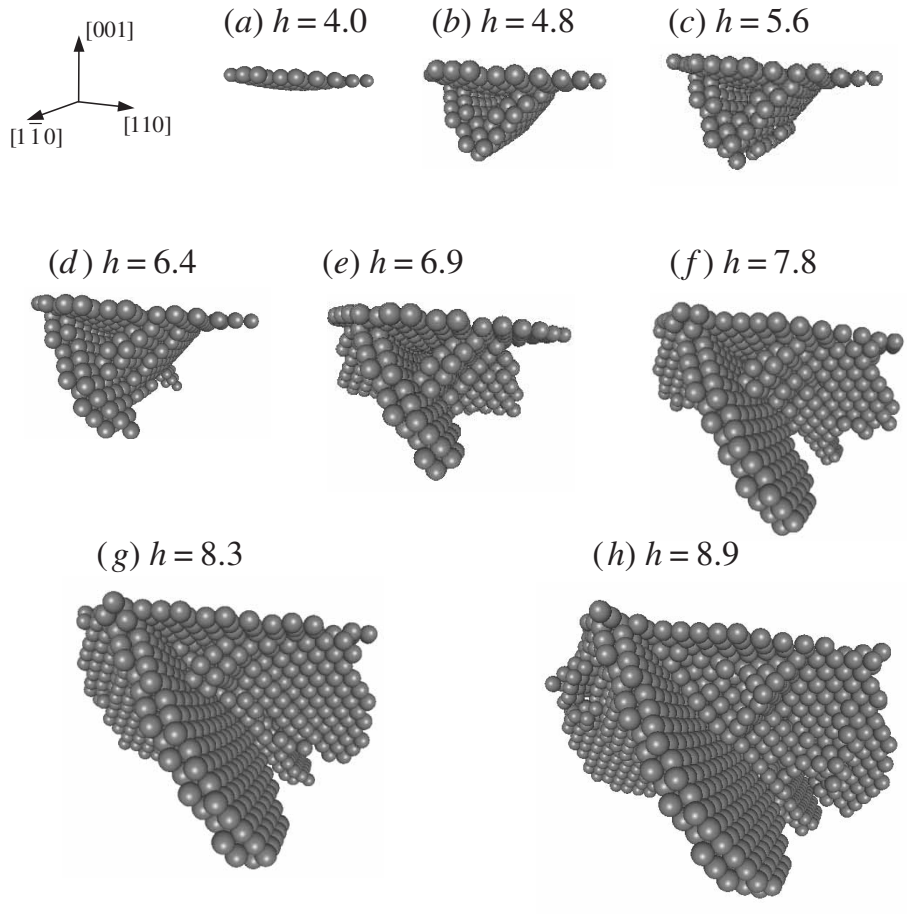

Figure 4. Microstructure evolution beneath the contact surface corresponding to the inflection points in figure 2: (*a*) a piece of surface elastically deformed prior to point 1; (*b*) point 1, where the formation and growth of Shockley partials and their interaction to form a Lomer–Cottrell lock; (*c*) appearance of faulted loops, leading to the deflection near point 2; (*d*) growth of the faulted loop and the bow-out of the unlocked segment on (111) from lock 1 between points 2 and 3; (*e*) formation of lock 2 and lock 3 perpendicular to lock 1 at point 3; (*f*) configuration after point 4, showing the bow-out of the unlocked segment in lock 2 and lock 3; (*g*) configuration at the beginning of the large deviation of point 5; (*h*) configuration just after point 5.

Figure 4 presents a sequence of atomic configurations, in which atoms with slip vectors having a magnitude $|\mathbf{s}^{\alpha}|$ ranging from 0.1 to 3.0 Å are identified. The sequence describes the development of the dislocation structure during indentation at various inflection points in figure 2.

Thus, figure 4(*a*) represents the deformed surface of the specimen under the indenter at an indentation depth of 4.0 Å. The lack of specific features to indicate any presence of dislocations suggests that the Cu substrate is deforming elastically, corresponding to the early part of the loading curve, that is prior to point 1 in figure 2. As the pentration increases beyond a depth of about 4.8 Å (point 1 in figures 2 and 4(*a*)), a pair of Shockley partials is nucleated at the point of highest stress concentration beneath the contact surface, with (111) and ($\bar{1}\bar{1}$1) slip planes

(figure 5(*a*)). The Shockley pair grows to intersect with the surface and with each other, forming a stair-rod dislocation and a Lomer–Cottrell lock (lock 1) (figures 4(*b*) and 5(*b*)). In the schematic diagram in figure 6(*a*), the locked segment bc is of pure edge character, formed from the dislocation reaction $\frac{1}{6}a[\bar{1}\bar{1}2] + \frac{1}{6}a[\bar{1}\bar{1}\bar{2}] = \frac{1}{3}a[\bar{1}\bar{1}0]$ (a is the lattice constant of Cu). The unlocked and non-edge segments ab and cd (with Burgers vector $\frac{1}{6}a[\bar{1}\bar{1}2]$), be and cf (with Burgers vector $\frac{1}{6}a[\bar{1}\bar{1}\bar{2}]$) connect the locked segment bc to the surface. The slip that occurs during the formation of lock 1 produces the minor yield at point 1 (figure 2). After the lock is formed, the crystal hardens, as reflected by the resumption of load increase. We note that, as the indentation depth increases, the contact area also increases beyond the lock where the deformation strain is smaller and remains in the elastic regime. Further displacement of the indenter is thus accommodated only partly plastically, by the glide of the non-edge and unlocked components in the form of bow-outs, causing the faulted region to expand along the ⟨110⟩ direction (figures 4 and 6). The balance of the deformation occurs elastically. This explains the complex quasi-elastic behaviour of the displacement–load curve.

The foregoing description is similar to simulation results reported in the literature, such as the formation of dislocation loops off the indenter axis (Kelchner *et al.* 1998), the nucleation of Shockley partials and stair-rod locks (Rodríguez de la Fuente *et al.* 2002) in Au, and the development of the pyramid defect structure on {111} faulted planes with edges of stair-rod nature (Gannepalli and Mallapragada 2002) found using a truncated pyramid indenter.

Although the tip of the indenter is perfectly spherical, Shockley partials form on only two of the four possible {111} slip planes in our simulation, despite the

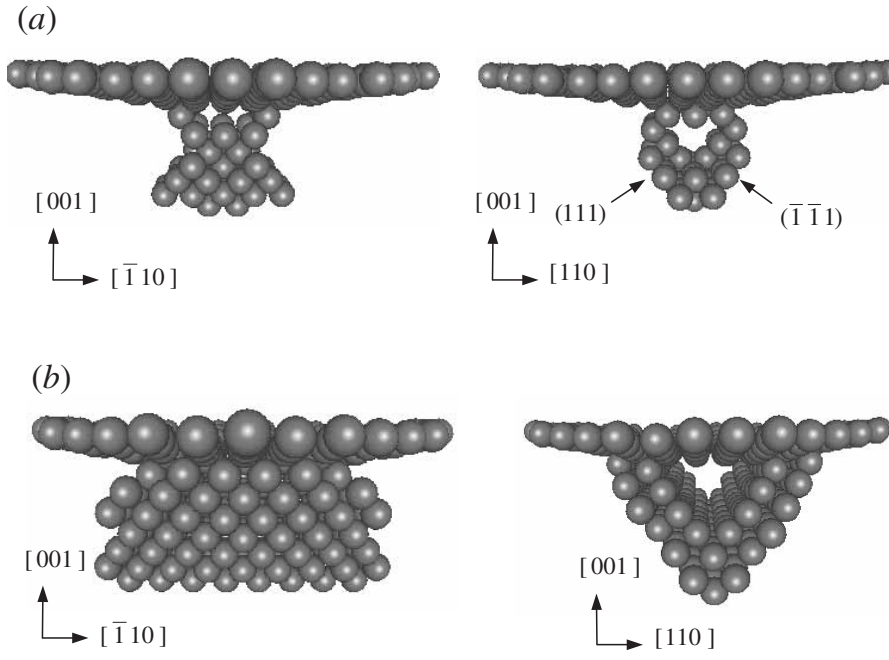

Figure 5. Formation of lock 1: (*a*) a pair of Shockley partials nucleate at the high stress region beneath the contact surface; (*b*) the partials grow and interact to form a stair-rod dislocation and the Lomer–Cottrell lock.

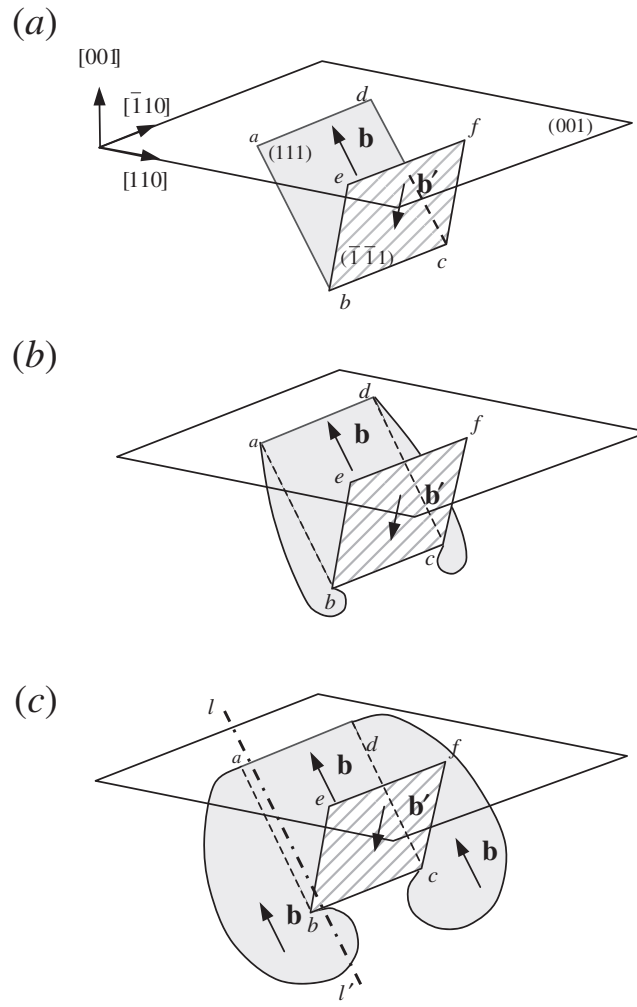

Figure 6. Schematic diagram of the bow-out of dislocation loops from lock 1 ($\mathbf{b} = \frac{1}{6}a[\bar{1}\bar{1}2]$; $\mathbf{b}' = \frac{1}{6}a[\bar{1}\bar{1}\bar{2}]$).

symmetry of the load. This symmetry-breaking occurrence is typical of bifurcations, and is due to the stochastic nature of nucleating events at finite temperatures.

The presence of the lock restricts the plastic flow of the material inside the wedged-shape region bounded by the two {111} slip planes and therefore hardens the material inside the wedge. The load transmitted by the indenter through the wedge creates a stress concentration at its tip, which generates, at a sufficiently large load, the proper condition for the nucleation of a pair of faulted loops (figure 7), with Burgers vectors $\frac{1}{6}a[\bar{1}\bar{1}2]$ on the (111) plane and $\frac{1}{6}a[\bar{1}\bar{1}\bar{2}]$ on the ($\bar{1}\bar{1}$1) plane, which grow along both sides of the wedge, producing the shear that allows the wedge to slip vertically downwards (compare the size of the fold between figures 8 (*a*) and (*b*)) under the load, thus producing the minor yield at point 2 (figure 2). As the faulted loops grow (figure 7 and figures 8 (*a*) and (*b*)), the thickness of the 'wall' of lock 1 changes from two atomic layers (intrinsic fault) to three (extrinsic fault). When the faulted loop reaches the surface, the quasi-elastic behaviour resumes.

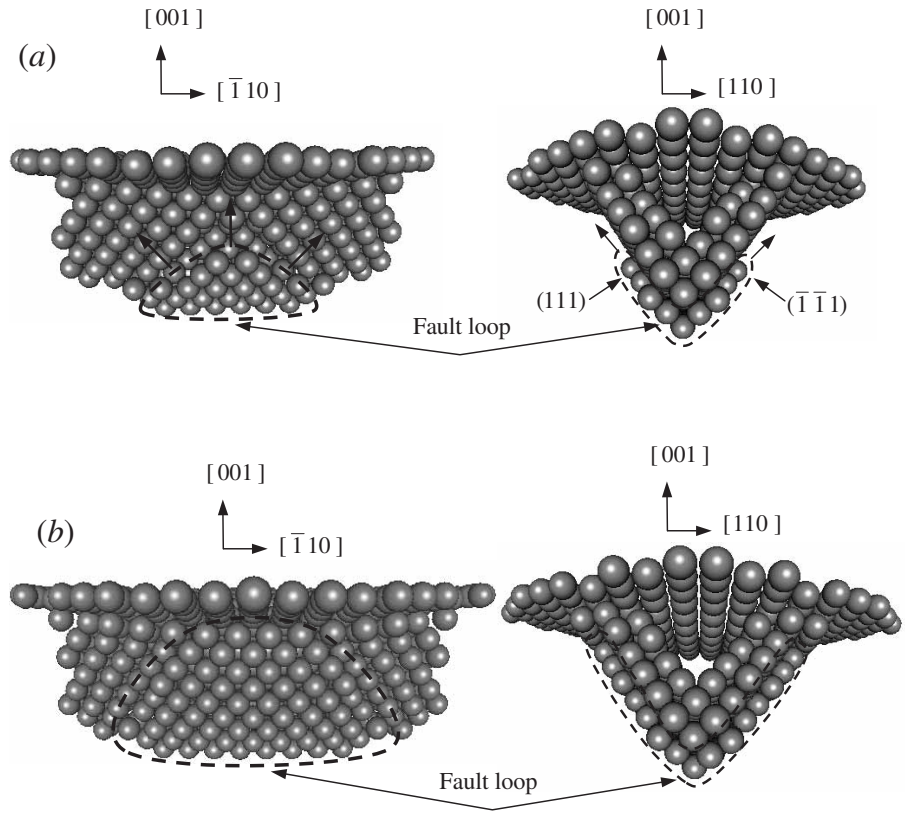

Figure 7. Formation of faulted loops on the side of lock 1: (*a*) the faulted loops begin to nucleate; (*b*) fault loops grow and come to a stop.

When the contact area becomes larger as the loading continues, the increase in local stress forces the unlocked non-edge segments ab and cd to bow out, expanding the faulted area on the (111) plane (figure 9 (*a*)). The resulting slip allows the local stress in the region above to relax. This starts the minor yield at point 3. On the other side of lock 1, away from the bow-out, the local stress continues to increase, causing the nucleation of a pair of Shockley partials that produces a Lomer–Cottrell lock (lock 2), in a similar way to the formation of lock 1 (figure 9 (*a*)). Subsequent to the nucleation and growth of lock 2, the stress increase on the diametrically opposite side across lock 1 causes the nucleation of a similar pair of partials, eventually forming lock 3 (figure 9 (*b*)). Both plastic processes contribute to the minor yield at point 3.

The displacement at point 3 is 0.13 Å, twice that of point 1 (0.06 Å). The larger slip distance can be seen from the larger sizes of lock 2 and lock 3, compared with lock 1. After the formation of lock 2 and lock 3, the yielding is interrupted and the load–displacement curve resumes its quasi-elastic behaviour between points 3 and 4. At this point, the microstructure beneath the indenter is made up of three locks, namely lock 1, lock 2 and lock 3, forming a cross. At the same strain rate, different parts of the surface deform via different mechanisms, some elastically, some via the dislocation bow out on the (111) plane and some via the nucleation and growth of Shockley partials, at high stress concentration points. The resultant effect produces the quasi-elastic behaviour on the load–displacement curve between points 3 and 4.

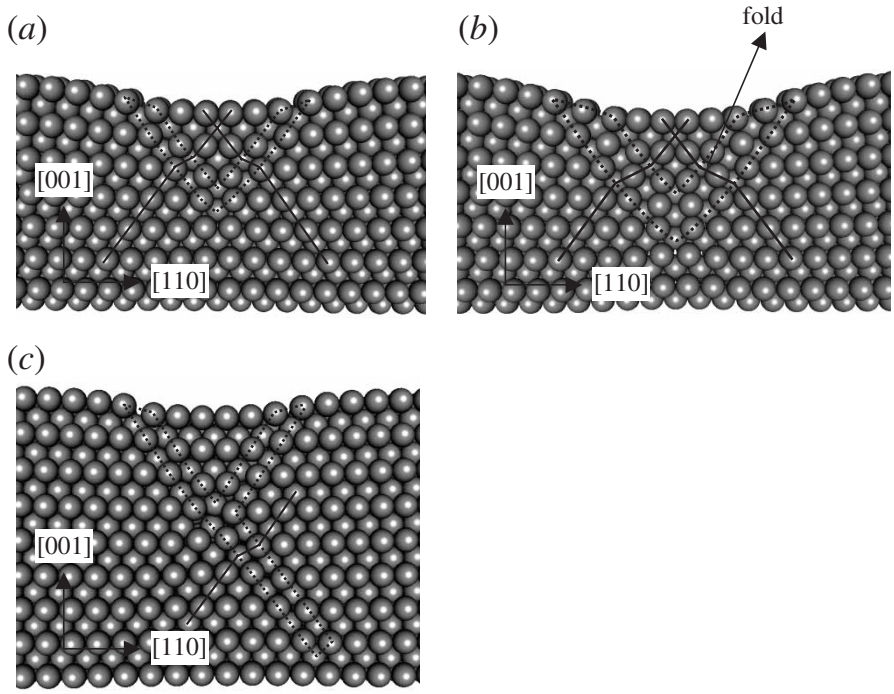

Figure 8. (*a*), (*b*) The cross-sections of the $(\bar{1}10)$ plane across the indenter axis, corresponding to figures 5 (*b*) and 7 (*b*) respectively; (*c*) cross-section of the $(\bar{1}10)$ plane across the chain line $11'$ in figure 6 (*c*), snapshot between points 3 and 4 in figure 2.

Beyond point 4, the expansion of the contact area drives the non-edge segments on lock 2 and lock 3 to bow out on the $(\bar{1}11)$ faulted plane, producing the major plastic deformation at point 5. The large excursions beyond point 5 correspond to the usual cold-working process, in which dislocations are generated (load drop), interact and form locks (load raise). We also note that, up to point 5 where major plasticity starts to occur, the locks remain intact and act as dislocation sources.

§ 3. Experimental interpretation

Feng and Ngan (2001) and Chiu and Ngan (2002) observed the time-delayed occurrence of pop-in below the spontaneous pop-in load during their nanoindentation experiments (figures 10 (*a*) and (*b*)). In the following, we argue that the formation of the Lomer–Cottrell lock prevents the further slip of the partial dislocations on the {111} planes and may thus offer a better explanation for the experimental observation.

In these experiments, the indentation was performed with a large and well-annealed Al crystal using a Berkovich tip. The load P was first ramped to 120 μN and held for 10 min, followed by unloading (figure 10 (*a*)). No plastic deformation could be detected from the displacement response after this cycle. The load was then reapplied at a higher level of 200 μN. This time a pop-in occurred after a holding time of about 400 s, as shown by the occurrence of a load drop and a surge in indenter displacement h. The loading and displacements as functions of time are shown in figure 10 (*a*), and the corresponding load–displacement relation is shown in figure 10 (*b*).

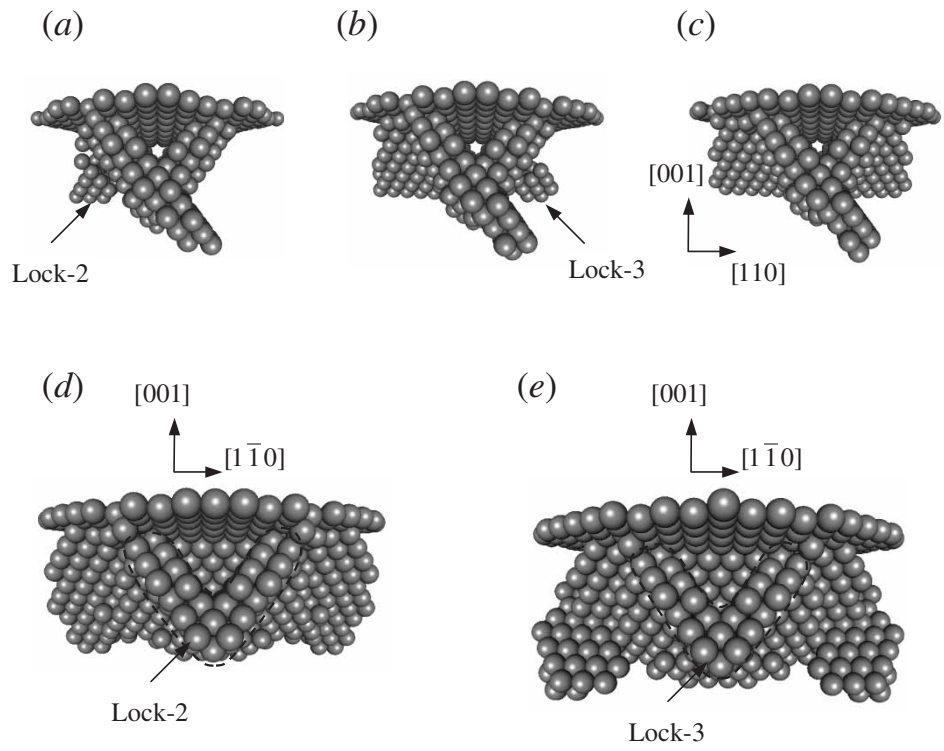

Figure 9. The formation process of lock 2 and lock 3: (*a*)–(*c*) the nucleation and growth of lock 2 and lock 3; (*d*), (*e*) side views of lock 2 and lock 3.

The time-delay occurrence of pop-in cannot be explained by homogeneous shear loop nucleation, because the activation energy involved would be much too large (Chiu and Ngan 2002). Some dislocations might have been generated during the holding time before pop-in, and these were either locked or existed in some form of stable state maintained by the load. Using line-tension arguments, Chiu and Ngan (2002) proposed that a small shear loop of up to a few Burgers vectors in size could be maintained in stable equilibrium by the load. However, the line tension model suggested is not likely to be sufficiently accurate at the small dimensions involved.

The simulation results here suggest the stair-rod formation to be a more plausible mechanism for the existence of a stable dislocation structure. Thus, at a small load, a sizeable pop-in does not occur spontaneously because the free loops are held back by the stair-rod dislocations, as shown in figures 4 (*b*)–(*h*). Upon removal of the load, the image force may very probably unzip the locked dislocation structure, leaving little or no residual deformation or dislocation debris. However, if the load is held for an extended time period, as the stair-rod dislocation is of an edge type, it may climb by pipe diffusion or other means. The proximity to the free surfaces and the large stress levels involved should greatly enhance the climb rate compared with those under the bulk condition. The dislocation structure may therefore expand, albeit slowly, with time, and a critical configuration may be surpassed so that an avalanche of dislocation slip and/or cross-slip activities may follow, yielding a sizeable pop-in.

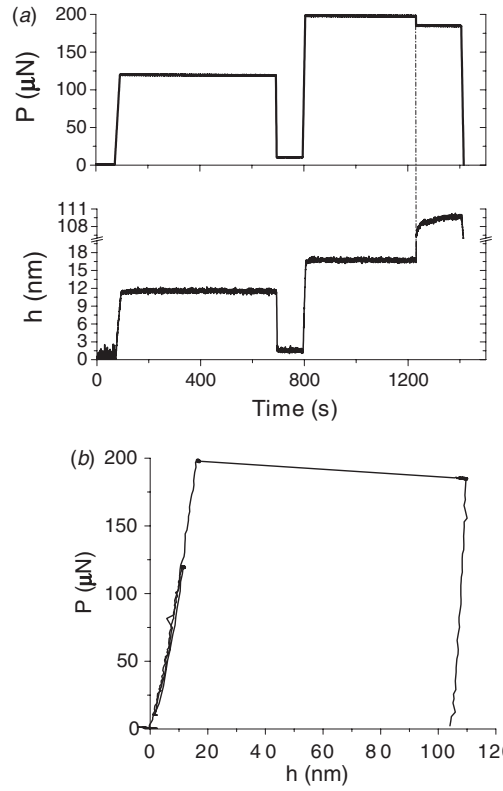

Figure 10. Constant-load experiment in Al at loads below the spontaneous pop-in value: (*a*) load schedule (upper curve) and displacement response (lower curve); (*b*) the corresponding load–displacement curve.

§4. Summary and conclusions

In this paper, the microstructure origin of the elastic–plastic deformation due to nanoindentation on the (100) surface of a Cu substrate is studied using MD simulation. For small indentation depths, the response is elastic but is found to deviate from the Hertzian solution. This has been shown to be mostly due to the small tip radius used in the simulation. For larger indentation depths, the deformation is mechanistically complex, and the ensuing dislocation structure is inhomogeneous. Even with the same strain rate, different mechanisms are found to be responsible for the deformation of different parts of the contact surface, some elastically, some via the dislocation bow-out and some via the nucleation and growth of Shockley partials and their subsequent interaction to form locks. The combined effect accounts for the observed complexity of the quasi-elastic behaviour, with interspersed minor yields on the load–displacement curve.

Experimentally, the stair-rod lock formation may provide a more satisfactory explanation to the observed time-delayed occurrence of pop-in below the spontaneous pop-in load.

Acknowledgement

The authors are grateful for funding support from the Hong Kong Research Grant Council PolyU5167/01E, PolyU5177/02E.

References

Brostow, W., Chybicki, M., Laskowski, R., and Rybicki, J., 1998, *Phys. Rev.* B, **57**, 13 448.

Chiu, Y. L., and Ngan, A. H. W., 2002, *Acta mater.*, **50**, 1599.

Clarke, A. S., and Jonsson, H., 1993, *Phys. Rev.* B, **47**, 3975.

Corcoran, S. G., Colton, R. J., Lilleodden, E. T., and Gerberic, W. W., 1997, *Phys. Rev.* B, **55**, 16 057.

Christopher, D., Smith, R., and Richter, A., 2001, *Nanotechnology*, **12**, 372.

Doyama, M., and Kogure, Y., 1999, *Comput. Mater. Sci.*, **14**, 80.

Feng, G., and Ngan, A. H. W., 2001, *Scripta mater.*, **45**, 971.

Fraxedas, J., Garcia-Manyes, S., Gorostiza, P., and Sanz, F., 2002, *Proc. natn. Acad. Sci. USA*, **99**, 5228.

Gane, N., and Bowden, F. P., 1968, *J. appl. Phys.*, **39**, 1432.

Gannepalli, A., and Mallapragada, S. K., 2002, *Phys. Rev.* B, **66**, 10 4103.

Gerberich, W. W., Tymiak, N. I., Grunlan, J. C., Horstemeyer, M. F., and Baskes, M. I., 2002, *J. appl. Mech.*, **69**, 433.

Gouldstone, A., Koh, H. J., Zeng, K. Y., Giannakopoulos, A. E., and Suresh, S., 2000, *Acta mater.*, **48**, 2277.

Kelchner, C. L., Plimpton, S. J., and Hamilton, J. C., 1998, *Phys. Rev.* B, **58**, 11 085.

Kiely, J. D., and Houston, J. E., 1998, *Phys. Rev.* B, **57**, 12588.

Kiely, J. D., Hwang, R. Q., and Houston, J. E., 1998, *Phys. Rev. Lett.*, **81**, 4424.

Kiely, J. D., Jaraush, K. F., Houston, J. E., and Russell, P. E., 1999, *J. Mater. Res.*, **14**, 2219.

Kracke, B., and Damaschke, B., 2000, *Appl. Phys. Lett.*, **77**, 361.

Kramer, D. E., Yoder, K. B., and Gerberich, W. W., 2001, *Phil. Mag.* A, **81**, 2033.

Krenn, C. R., Roundy, D., Cohen, M. L., Chrzan, D. C., and Morris, J. W., Jr, 2002, *Phys. Rev.* B, **65**, 134 111.

Kulp, D. T., Ackland, G. J., Sob, M., Vitek, V., and Egami, T., 1993, *Modelling Simulation Mater. Sci. Engng*, **1**, 315.

Li, J., Van Vliet, K. J., Zhu, T., Yip, S., and Suresh, S., 2002, *Nature*, **418**, 307.

Liu, Y., and Ngan, A. H. W., 2001, *Scripta mater.*, **44**, 237.

Minor, A. M., Morris, J. W., Jr, and Stach, E. A., 2001, *Appl. Phys. Lett.*, **79**, 1625.

Rodríguez de la Fuente, O., Zimmerman, J. A., González, M. A., de la Figuera, J., Hamilton, J. C., Pai, W. W., and Rojo, J. M., 2002, *Phys. Rev. Lett.*, **88**, 36 101.

Swadener, J. G., George, E. P., and Pharr, G. M., 2002, *J. Mech. Phys. Solids*, **50**, 681.

Zimmerman, J. A., Kelchner, C. L., Klein, P. A., Hamilton, J. C., and Foiles, S. M., 2001, *Phys. Rev. Lett.*, **87**, 165 507.